THE JOURNAL OF BIOLOGICAL CHEMISTRY
© 2005 by The American Society for Biochemistry and Molecular Biology, Inc.

Vol. 280, No. 8, Issue of February 25, pp. 7218–7227, 2005
Printed in U.S.A.

Structures of APRIL-Receptor Complexes

LIKE BCMA, TACI EMPLOYS ONLY A SINGLE CYSTEINE-RICH DOMAIN FOR HIGH AFFINITY LIGAND BINDING*[S]

Received for publication, October 14, 2004, and in revised form, November 9, 2004
Published, JBC Papers in Press, November 12, 2004, DOI 10.1074/jbc.M411714200

Sarah G. Hymowitz‡, Darshana R. Patel‡, Heidi J. A. Wallweber‡, Steven Runyon‡, Minhong Yan§, JianPing Yin‡, Stephanie K. Shriver‡, Nathaniel C. Gordon‡, Borlan Pan‡, Nicholas J. Skelton¶, Robert F. Kelley‡, and Melissa A. Starovasnik‡‖

From the Departments of ‡Protein Engineering, §Molecular Oncology, ¶Medicinal Chemistry, and ‖Immunology, Genentech, Inc., South San Francisco, California 94080

TACI is a member of the tumor necrosis factor receptor superfamily and serves as a key regulator of B cell function. TACI binds two ligands, APRIL and BAFF, with high affinity and contains two cysteine-rich domains (CRDs) in its extracellular region; in contrast, BCMA and BR3, the other known high affinity receptors for APRIL and BAFF, respectively, contain only a single or partial CRD. However, another form of TACI exists wherein the N-terminal CRD is removed by alternative splicing. We find that this shorter form is capable of ligand-induced cell signaling and that the second CRD alone (TACI_d2) contains full affinity for both ligands. Furthermore, we report the solution structure and alanine-scanning mutagenesis of TACI_d2 along with co-crystal structures of APRIL/TACI_d2 and APRIL/BCMA complexes that together reveal the mechanism by which TACI engages high affinity ligand binding through a single CRD, and we highlight sources of ligand-receptor specificity within the APRIL/BAFF system.

Members of the tumor necrosis factor (TNF)[1] superfamily of ligands and their receptors (TNFR) are critical regulators of the adaptive immune system. The ligands are type II transmembrane protein cytokines that have diverse and, at times, opposing effects on various immune cell types including acting as costimulatory molecules, apoptotic agents, and growth factors (1). APRIL (also known as TNSF13A, TALL-2, and TRDL-1) is a TNF ligand that is overexpressed by some tumors and stimulates tumor cell growth (2); however, its function in normal biology is less clear (3). APRIL is most similar in sequence to the B cell activation factor, BAFF (also known as TNSF13B, BLyS, TALL-1, THANK, and zTNF4). BAFF is essential for the normal development of mature B cells via signaling through the divergent TNFR BR3 (also known as BAFF-R) (4–9).

Despite their differences in function, APRIL and BAFF are linked as they both can bind the TNFRs TACI and BCMA (10–13). However, TACI alone serves as a high affinity receptor for both APRIL and BAFF because monovalent BCMA binds BAFF only weakly (14, 15). TACI functions, at least in part, as a negative regulator of BAFF function given that loss of TACI expression results in the overproduction of B cells and autoimmunity in mice (16, 17). The role of BCMA is less clear, although it appears to be important for the survival of long lived plasma cells (18). A third APRIL-specific receptor may exist as APRIL can stimulate cells that express neither BCMA nor TACI (11).

The extracellular domain of a typical TNFR contains multiple copies of so-called ~40-residue cysteine-rich domains (CRDs), which bind in the monomer-monomer interfaces of a trimeric ligand (19). TACI is a member of the TNFR superfamily possessing two CRDs; interestingly however, the two CRDs of TACI are more similar to each other (~50% sequence identity) than is typical in the TNFR family (20). BCMA and BR3, in contrast, are unusually small TNFRs as they contain only a single or partial CRD, respectively. The only other known TNFRs possessing just a single CRD are FN14 (21) and the *Drosophila* TNFR, Wengen (22). All human APRIL or BAFF receptor CRDs, including both domains of TACI, share a common sequence feature, the so-called DXL motif, which consists of a conserved 6-residue sequence (Phe/Tyr/Trp)-Asp-Xaa-Leu-(Val/Thr)-(Arg/Gly). This motif is required for binding to either APRIL or BAFF (15, 23–25). Crystal structures of BAFF bound to BCMA, BR3, or a peptide presenting the DXL motif in a β-hairpin scaffold show that this receptor motif binds in a hydrophobic pocket and interacts with two conserved arginine residues on the BAFF surface (23, 24, 26). The structure of APRIL alone was recently shown to be very similar to that of BAFF and indicates that the DXL binding site is conserved in the two ligands (27–31). Thus, a similar mode of ligand-receptor interaction via the DXL site is expected for APRIL-receptor complexes; however, ligand binding specificity of BR3 and BCMA appears to be determined by interactions outside this common motif (15, 23, 26).

Since both CRDs of human TACI contain the DXL motif and have been shown qualitatively to interact with BAFF (24), questions remain as to whether each domain actively contributes to ligand binding in the context of the full-length receptor or whether only one is exploited for optimal ligand binding; and if only a single domain is sufficient to achieve high affinity

* The costs of publication of this article were defrayed in part by the payment of page charges. This article must therefore be hereby marked "*advertisement*" in accordance with 18 U.S.C. Section 1734 solely to indicate this fact.

[S] The on-line version of this article (available at http://www.jbc.org) contains Tables S1–S4 and Fig. S1.

** To whom correspondence should be addressed: Dept. of Protein Engineering, 1 DNA Way, South San Francisco, CA 94080. E-mail: star@gene.com.

[1] The abbreviations used are: TNF, tumor necrosis factor; APRIL, a proliferation-inducing ligand; BAFF, B cell activation factor; BCMA, B cell maturation antigen; BR3, BLyS/BAFF receptor 3; CAPS, 3-(cyclohexylamino)propanesulfonic acid; CRD, cysteine-rich domain; HSQC, heteronuclear single quantum coherence; MES, 4-morpholineethanesulfonic acid; NFκB, nuclear factor-κB; NOE, nuclear Overhauser effect; NOESY, NOE spectroscopy; PEG, polyethylene glycol; r.m.s.d., root mean square deviation; TACI, transmembrane activator and CAML interactor; TNFR, member of TNF receptor superfamily.

binding, whether APRIL and BAFF favor the same or different TACI domains. Alternatively, both CRDs together could contribute to ligand binding as is typically observed for multidomain TNFRs (19). Additionally, Kim and co-workers (24) have postulated that TACI might span adjacent BAFF trimers with its two CRDs.

To understand whether TACI functions more like a multidomain TNFR or like the small and more specific receptors BR3 and BCMA, we have characterized the APRIL-TACI interaction using cell-based, biochemical and structural studies. We show that an alternative splice form of TACI lacking the N-terminal CRD is still functional for signaling. Furthermore, we found that only the membrane-proximal CRD (TACI_d2) is required for high affinity binding to either APRIL or BAFF. The solution structure of TACI_d2 reveals a compact domain similar to that of BCMA; however, combinatorial alanine-scanning mutagenesis identified additional ligand binding determinants unique to TACI_d2. The co-crystal structures of APRIL-TACI_d2 as well as APRIL-BCMA complexes show remarkably large interfaces and highlight key differences among the APRIL and BAFF receptors which influence ligand binding affinity and specificity. Thus, despite the presence of two CRDs in the extracellular domain of TACI, only a single domain is employed for both APRIL- and BAFF-dependent signaling.

EXPERIMENTAL PROCEDURES

Protein Production—Murine APRIL was produced as described previously (28). Murine APRIL was used throughout the study because it is better behaved biochemically than recombinant human APRIL. Differences between murine and human APRIL lie outside the receptor binding site (Ref. 28 and see below), thus, similar receptor binding affinities for murine and human APRIL are expected. Human TACI_d1d2 (residues 21–116) and TACI_d1 (residues 32–67) were produced from baculovirus using essentially the same procedure. DNA coding for the TACI fragments followed by a C-terminal His tag were subcloned into the baculovirus transfer vector pAcGP67B (Pharmingen). After transfection and viral amplification in Sf9 cells, proteins were expressed and secreted from Hi5 cells grown at 27 °C. 50 mM Tris, pH 8.0, 1 mM $NiCl_2$, 5 mM $CaCl_2$, and 1 μM phenylmethylsulfonyl fluoride were added to the culture medium, the pH was adjusted to 7.5, and the medium was filtered prior to loading on a nickel-nitrilotriacetic acid (Qiagen) column. After elution with imidazole, relevant fractions were pooled and purified further on a Superdex-75 (S-75) sizing column.

For production of human TACI_d2, DNA encoding TACI residues 58–109 was subcloned into the pET32a expression vector (Novagen), creating a fusion protein consisting of an N-terminal thioredoxin domain followed by a His tag, thrombin cleavage site, then TACI_d2. Protein was expressed in *Escherichia coli* Origami (DE3) cultures grown at 37 °C in LB medium for unlabeled protein, or M9 minimal medium containing uniformly ^{13}C-labeled glucose and $[^{15}N]NH_4Cl$ to generate protein samples for NMR spectroscopy. After cultures grew to an A_{600} of 0.7, the temperature was lowered to 16 °C and expression induced overnight with 1 mM isopropyl 1-thio-β-D-galactopyranoside. Thioredoxin-TACI_d2 was purified over a nickel-nitrilotriacetic acid column. Thioredoxin was removed by thrombin cleavage, then TACI_d2 was purified further either using reverse phase high performance liquid chromatography for the NMR samples or on an S-75 column in 20 mM CAPS, pH 9.7, 400 mM NaCl (buffer A) for crystallography. Human BAFF, human BCMA-Fc, and human BCMA-Z were expressed and purified as described previously (15). The identities of all purified proteins were verified by N-terminal sequencing and mass spectrometry.

Competitive Binding Assays—A BIAcore 3000 instrument (BIAcore, Inc.) was used to measure ligand-receptor interactions in solution using a competitive binding format. BCMA-Fc was coupled to a CM4 sensor chip, using the amine coupling protocol supplied by the manufacturer, at a high density (4,500 resonance units) so the initial rate of binding was linearly dependent on free ligand concentration. The chip surface was regenerated between sample injections by washing with 10 mM HCl. Fixed ligand concentrations (12.5 nM BAFF; 50 nM thioredoxin-APRIL) in the presence of varying receptor concentrations were incubated for 2 h. Samples were then passed over the BCMA-Fc-coupled surface. A linear fit of the initial on-rate of the observed sensorgrams was used to calculate the concentration of free ligand. The IC_{50} values were calculated using a four-parameter curve fit of the fractional rate of binding free ligand as a function of competing receptor concentration. Receptors were also tested for binding either to APRIL or to BAFF in a competition enzyme-linked immunosorbent assay as described previously (15), except that BAFF binding assays utilized biotinylated BR3-ECD rather than biotinylated "mini-BR3" (23) as the probe.

Phage Display of TACI_d2—DNA encoding TACI_d2 (residues 68–109) was subcloned into the phagemid BCMA2-g3 described previously (15). TACI_d2-g3 was used to prepare three "shotgun alanine" scanning libraries essentially as described previously (32). Each library contains shotgun codons at unique positions: library one has 11 shotgun codons at positions 72, 73, 74, 75, 76, 77, 78, 80, 81, 83, and 85; library two has 13 shotgun codons at positions 79, 81, 82, 84, 87, 88, 91, 92, 94, 95, 96, 97, 98; and library three has 8 shotgun codons at positions 99, 102, 103, 105, 106, 107, 108, and 109. Libraries were sorted for binding against APRIL, BAFF or anti-tag antibody (3C8-2F4 Genentech, Inc.), and sequences of phage clones were analyzed as described previously (15). For APRIL binding, 71, 40, and 54 sequences were analyzed from libraries one, two and three, respectively. For BAFF binding, 70, 50, and 53 sequences were analyzed for libraries one, two and three, respectively. For the display selection, at least 47 sequences were analyzed for each library. The number of times a particular amino acid was found at each position was tabulated, and the normalized wild-type/mutant functional ratio, *F*, was calculated for each position as described previously (33) (see Table S3). *F* represents a measure of the apparent effect of mutation of a given residue on binding affinity, with values >1 representing deleterious mutations. Because of the relatively small number of sequences analyzed, only those mutations showing a greater than 10-fold effect (i.e. $F > 10$) are considered significant.

NMR Spectroscopy—NMR samples typically contained ~1 mM protein, 50 mM sodium phosphate, pH 7.2, 50 mM NaCl, 0.1 mM sodium azide, and 50 μM 1,4-dioxane as an internal chemical shift reference standard in 90% H_2O, 10% D_2O. A "100% D_2O" sample was prepared by lyophilization and resuspension in 99.995% D_2O. NMR spectra were acquired at 17 °C on a Bruker DRX600 spectrometer equipped with a triple resonance cryoprobe. All NMR data were processed using FELIX (version 2000.1; Accelrys, San Diego) and analyzed using the program Sparky (version 3.11, Goddard and Kneller, University of California, San Francisco). Backbone resonance assignments of TACI_d2 were obtained from double and triple resonance experiments in H_2O solution, as described previously (34 and see Table S1). Stereospecific assignments of leucine methyl groups were obtained from a ^1H-^{13}C HSQC spectrum of a 15% ^{13}C-labeled sample (35). Backbone dynamics were investigated by analyzing the steady state $[^1H]$-^{15}N-NOE as described previously (23, 36).

Distance restraints were obtained from analysis of the following NOESY spectra: three-dimensional ^1H-^{15}N-edited NOESY (200 ms mixing time) measured in H_2O; three-dimensional ^{13}C-edited NOESY (150 ms mixing time) measured in D_2O; and two-dimensional ^1H-^1H NOESY (150 ms mixing time) measured in D_2O. NOE peaks were picked manually, and NOE assignments were obtained using the automated NOE assignment program CANDID (37) followed by several rounds of structure calculation and manual restraint checking. Dihedral angle restraints were obtained from analysis of three-dimensional ^{15}N-^1H HNHB and three-dimensional ^{13}C-edited NOESY-HSQC (50 ms mixing time) spectra. Backbone dihedral angle restraints were obtained from analysis of backbone chemical shifts with the program TALOS (38). Dihedral restraints were applied for good fits to the chemical shifts with the allowed range of ±30° (for φ), ±40° (for ψ). The final structures were calculated using the program CNX (version 2002; Accelrys). 100 structures were calculated using torsion angle dynamics followed by Cartesian dynamics and minimization. The 20 structures with the lowest restraint violation energy were chosen to represent the solution structure (Table S2).

One of the differences between the NMR ensemble of TACI_d2 and the crystal structure of the same domain bound to APRIL is the conformation of the C-terminal disulfide (Cys^{83}/Cys^{104}). Thus, a separate set of structures was calculated using dihedral angle restraints to force the disulfide bonds to adopt the conformation observed in the crystal structure (−60 ± 20° for χ_1, −60° ± 20° for χ_2, and −90 ± 20° for χ_3) in addition to the NMR-derived restraints. Using these additional restraints had the desired effect on disulfide bond geometry yet did not introduce significant NOE or dihedral angle restraint violations (r.m.s.d. values of 0.008 Å and 0.36°, respectively) or noticeable changes in the backbone conformation (0.58 ± 0.09 Å backbone r.m.s.d. for residues 76–104 to mean structure with NMR-derived restraints only). Thus the difference in conformation seen for the Cys^{83}/Cys^{104} disulfide bond may result from the lack of experimental dihedral angle restraints

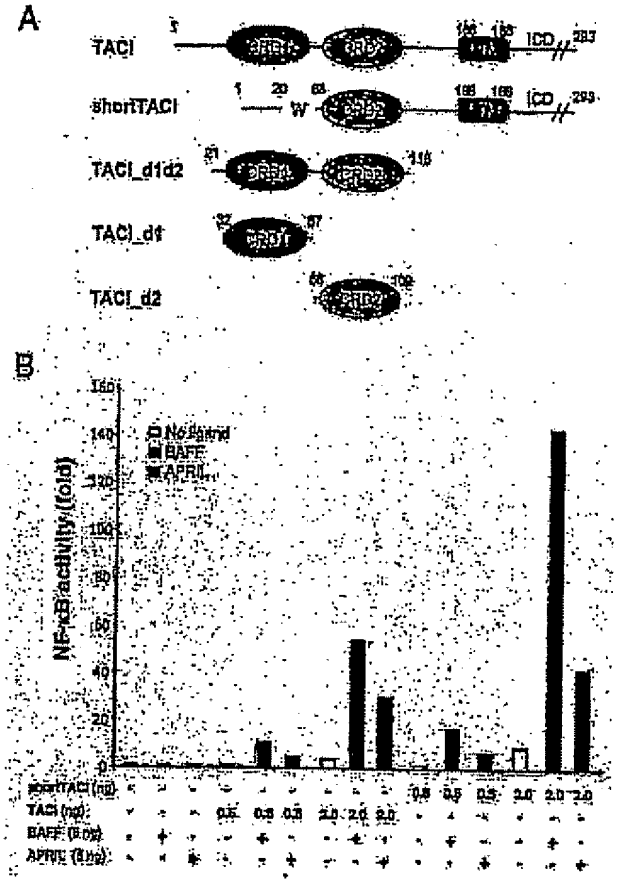

FIG. 1. Domain structure and function of TACI variants. *A*, schematic of the domain structure of full-length TACI, its alternative splice variant shortTACI, and the recombinant proteins used in this study. *B*, shortTACI can induce NFκB activation through either APRIL or BAFF. Human 293T cells were cotransfected with the indicated amounts of expression plasmids along with 250 ng of ELAM-luciferase reporter gene plasmid and 25 ng of pRL-TK. 20 h after transfection, reporter gene activity was determined with the dual luciferase reporter assay system (Promega).

and the imprecise nature of the NOE restraints in this region.

Production and Crystallization of APRIL-Receptor Complexes—APRIL (15, 28) and TACI_d2 were combined in buffer A, purified as a complex over an S-75 column in buffer A, and concentrated to 1 mg/ml. Crystals grew at 19 °C from sitting drops containing 1 μl of protein and 1 μl of reservoir solution (70% methylpentane diol, 0.1 M Hepes, pH 7.5). The complex of APRIL and BCMA-Z was first purified over an S-75 sizing column in buffer A, then Z-domain was removed by cleavage with endoproteinase Lys-C (EMD Biosciences), and the complex was repurified over the S-75 column. APRIL-BCMA fractions were concentrated to 8.4 mg/ml. Crystals grew at 19 °C from sitting drops containing 1 μl of protein and 1 μl of reservoir solution (0.1 M MES, pH 5.0, 5% PEG 8000, and 10% PEG 1000).

Crystallography—APRIL/TACI_d2 crystals were cryocooled without any additional cryoprotectant. The APRIL-BCMA crystals were first transferred to an artificial mother liquor containing 0.1 M MES, pH 5.0, 5% PEG 8000, 10% PEG 1000, 400 mM NaCl, and 10 mM CAPS, pH 9.7. Mother liquor was slowly exchanged for a cryoprotectant consisting of the mother liquor with 20% PEG 300 and then cooled by immersion in liquid nitrogen. A 1.9 Å data set of APRIL/TACI_d2 and a 2.35 Å data set of APRIL-BCMA were collected at 19BM at the APS. Processing of the APRIL/TACI_d2 data with HKL resulted in a data set with R_{sym} = 8.6% (35% in the 1.97–1.90 Å shell), 99.6% completeness, 6.5-fold redundancy, and $\langle I/\sigma I \rangle$ = 7.4 in space group $P2_12_12_1$, whereas processing of the APRIL-BCMA data with HKL (39) resulted in a data set with R_{sym} = 6.7% (43% in the 2.43–2.35 Å shell), 99.9% completeness, 9.4-fold redundancy, and $\langle I/\sigma I \rangle$ = 11.7 in space group $P6_1$ (Table S4). The structures were solved by molecular replacement with the program AMoRe using the structure of APRIL alone (PDB code 1U5Z (28)) as the search model for the APRIL/TACI_d2 data, and the refined APRIL trimer coordinates from that complex as the search model for the APRIL-BCMA data. Refinement of both structures was performed with the program REFMAC5 (40) and included TLS refinement and NCS restraints imposed separately on APRIL and the receptor, resulting in an R/R_{free} of 16.7/20.3% for the APRIL/TACI_d2 structure and an R/R_{free} of 17.8/21.2% for the APRIL-BCMA structure (Table S4).

RESULTS

"ShortTACI": An Alternatively Spliced Form of TACI Containing a Single CRD—As part of an attempt to find additional BAFF receptors through expression cloning (8, 41) we isolated a splice variant of human TACI wherein exon 2, which encodes the first CRD in the extracellular region, was replaced by a single residue. The polypeptide generated by this alternative splicing event (shortTACI) contains the first 20 residues of TACI, a tryptophan residue in place of 47 residues that encode CRD1, then the rest of the protein including CRD2, the transmembrane, and the intracellular regions (Fig. 1*A*). The identical splice variant was also reported in the public GenBank (accession number AAP57629). Previously we have shown that stimulation of TACI by its ligands APRIL and BAFF can lead to activation of NFκB *in vitro* (10). Interestingly, we found that shortTACI was capable of mediating NFκB activation by either APRIL or BAFF (Fig. 1*B*). The assay depends on cotransfection of the ligand and receptor, hence the extent of signaling observed will depend in part on the relative transfection efficiencies for each gene. Therefore, quantitative comparisons cannot

A

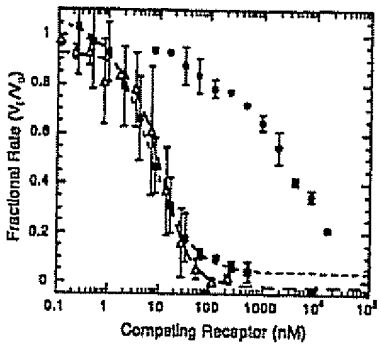

B

Competitor	APRIL IC_{50} (nM)	BAFF IC_{50} (nM)
TACI_d1d2	11 ± 8	1.3 ± 0.7
TACI_d1	2000	>100*
TACI_d2	5.9 ± 1.4	1.8 ± 1.3

FIG. 2. **APRIL and BAFF binding by TACI variants.** Competitive surface plasmon resonance experiments to measure binding to APRIL or BAFF were performed as described under "Experimental Procedures." *A*, competitive inhibition of APRIL binding to BCMA-Fc by TACI variants: TACI_d1 (*filled circles*), TACI_d2 (*filled squares*), TACI_d1d2 (*open triangles*). *B*, IC_{50} values for competitive binding to APRIL and BAFF are shown as the mean of two (TACI_d1) or three (TACI_d1d2, TACI_d2) independent experiments. An *asterisk* (*) indicates that an interaction was observed between TACI_d1 and BAFF, but the binding curve could not be fitted adequately to derive an accurate IC_{50} value.

be made from this experiment. However, the observation of BAFF- or APRIL-dependent NFκB activation by shortTACI indicates that TACI CRD1 is not required for ligand-dependent cell signaling (Fig. 1*B*).

TACI_d2 Is Sufficient for High Affinity Ligand Binding—Given that shortTACI containing only a single CRD was capable of ligand-dependent signaling, the abilities of the individual CRDs of TACI (TACI_d1, TACI_d2) and a construct containing both TACI CRDs (TACI_d1d2) were evaluated for their abilities to bind APRIL or BAFF (Fig. 1*A*). By surface plasmon resonance competition experiments, the 42-residue TACI_d2 fragment was found to have high affinity for both APRIL and BAFF (IC_{50} = 6 and 2 nM, respectively; Fig. 2). Moreover, the addition of CRD1 (in the context of the TACI_d1d2 fragment) did not confer additional affinity over that measured for TACI_d2 alone for either ligand. In contrast, the affinity of TACI_d1 was substantially weaker than that of TACI_d2, with IC_{50} values in the micromolar range, for both APRIL and BAFF (Fig. 2). Competitive enzyme-linked immunosorbent assays confirmed that TACI_d2 is sufficient for high affinity binding to both ligands, with no improvement in binding with TACI_d1d2 (data not shown).

These results are consistent with those reported previously, where Kim *et al.* (24) found that each domain of human TACI was capable of binding BAFF through its respective DXL motif (when measured in the context of Fc fusion proteins) and that mutation of both DXL motifs in full-length TACI was required to eliminate BAFF binding as detected qualitatively by coimmunoprecipitation. Our interpretation differs from Kim and co-workers (24), however, because of the finding that TACI_d2 has much higher ligand binding affinity than TACI_d1. Furthermore, the DXL motif is not conserved in murine TACI CRD1 (41). Therefore, in the context of the full-length receptor, these data suggest that the membrane-proximal CRD2 will occupy the DXL-receptor binding site on the ligand, with CRD1 providing minimal additional binding energy.

A

B

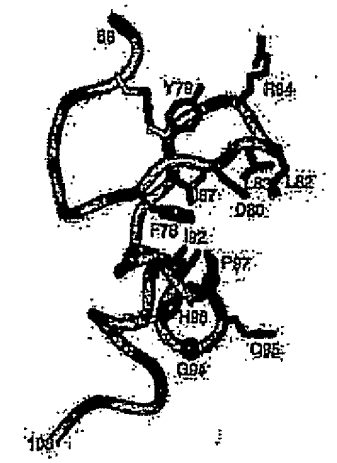

FIG. 3. **Solution structure of TACI_d2.** *A*, stereo view of the ensemble of 20 TACI_d2 models showing backbone (N, Cα, C atoms) of residues 68–108 and side chain heavy atoms for Cys^{71}/Cys^{86}, Cys^{89}/Cys^{100}, and Cys^{83}/Cys^{104}. Asp^{90}, Leu^{83}, and Arg^{84} are also shown to emphasize disorder of these residues compared with the crystal structure. The solution NMR models (*white* with *yellow* sulfur atoms) are superimposed (N, Cα, C atoms of residues 76–104) with the three TACI_d2 chains present in the asymmetric unit of the APRIL/TACI_d2 crystal structure (shades of *blue* with *orange* sulfur atoms). *B*, representative structure of TACI_d2. Residues important for binding to BAFF (*blue*), APRIL (*green*), or both (*pink*) based on shotgun alanine scanning ($F > 10$) are shown. Note that several of these side chains (Asp^{90}, Leu^{83}, Leu^{87}, and Glu^{95}) are exposed to solvent, and their side chain conformations are not well defined in the ensemble.

Solution Structure of TACI_d2—The solution structure of TACI_d2 was determined by NMR spectroscopy as described under "Experimental Procedures" and in the Supplemental material (Tables S1 and S2). The ensemble of the 20 structures of TACI_d2 having the lowest restraint violation energy (Fig. 3*A*) shows a well defined core between residues 76 and 105 (0.52 ± 0.08 Å average r.m.s.d. to the mean coordinates for N, C_α, C backbone atoms), with residues at the N and C termini being poorly defined. $[^1H]$-^{15}N heteronuclear NOE values indicate that residues at the extreme termini (residues 64–70 and 106–109) are highly flexible on the ps-ns time scale (Fig. S1).

The disorder of residues 71–76 in the ensemble is the result of a lack of restraints to define this region and likely also because of conformational heterogeneity on a μs-ms time scale given the broadness of many of the peaks for these residues. This region also adopts very different conformations in the three TACI_d2 chains present in the asymmetric unit of the APRIL/TACI_d2 crystal structure (see below; Fig. 3A).

The overall fold of TACI_d2 is similar to that observed previously for the related TNFR BCMA (26) and consists of two submodules: an N-terminal strand connected to a β-hairpin (residues 76–88) with a type I reverse turn containing the conserved DXL motif, and a short helix-loop-helix submodule consisting of a turn of 3_{10}-helix (h1, residues 89–92), an intervening loop, and a distorted C-terminal 3_{10}-helix (h2, residues 98–105). The disulfide bonding pattern is also similar to that of BCMA: one disulfide bond (Cys^{71}/Cys^{86}) connects the N terminus to the β-hairpin, and two disulfide bonds (Cys^{82}/Cys^{100}, Cys^{93}/Cys^{104}) connect h1 and h2.

The backbone of the conserved DXL loop is well defined (0.13 ± 0.02 Å backbone r.m.s.d. for residues 78–87) and superimposes nicely with that of both BCMA (r.m.s.d. 0.38 ± 0.04 Å for residues 13–22 of the eight copies of BCMA; 1OQD (26)) and BR3 (r.m.s.d. 0.56 Å for residues 24–33; 1OSX representative structure (23)). The aromatic side chain of Tyr^{79} is well ordered in the ensemble and is positioned above the hairpin. An equivalent aromatic residue is present in BCMA and BR3 (Phe^{14} in BCMA and Phe^{25} in BR3). Energetic studies of hairpin stability have suggested that a bulky hydrophobic or aromatic side chain at this position can stabilize hairpin structure (33, 43). There is a well ordered hydrophobic core formed by the side chains of Phe^{78}, Ile^{87}, Ile^{92}, and Pro^{97}. The side chain of His^{96} is also well defined and packs into the interior of the C-terminal submodule.

Mutational Analysis of TACI_d2—A combinatorial (shotgun) alanine scan (32) of TACI_d2 was used to determine the apparent contribution of individual amino acid side chains to the binding of either APRIL or BAFF. Three different libraries were generated to allow mutation of residues 72–109 (except positions where the wild-type residue is cysteine or alanine). Wild-type codons were replaced by shotgun alanine codons, allowing residues to vary as the wild-type amino acid or alanine. For positions where the wild-type residue is Arg, Asn, Gln, His, Ile, Leu, Phe, or Tyr, the shotgun codon allows two additional amino acid substitutions (32) (Table S3). Similar analyses for BR3 and BCMA binding to BAFF and/or APRIL were reported previously (15, 23).

A total of 12 TACI residues resulted in significant loss of affinity for APRIL and/or BAFF when mutated to alanine (Fig. 4). These residues map to a concave surface on the TACI_d2 structure and indicate that both submodules of TACI_d2 are important for ligand binding (Fig. 3B). Seven residues from the DXL hairpin showed significant effects, including both the D (Asp^{80}) and L (Leu^{82}), which are clearly essential for both APRIL and BAFF binding because the wild-type residue was always selected. Leu^{83} at the tip of the β-turn was also relatively intolerant to substitution by alanine for either APRIL or BAFF binding but was frequently replaced by valine, especially for binding BAFF (Table S3). Furthermore, a hydrophobic residue at position 87 is clearly important, as only isoleucine (the wild-type residue) or valine was selected for binding to both ligands. Residues from the C-terminal submodule including those from h1 (Ile^{92}) and the h1h2 loop (residues 94–97) also showed contributions to binding (Fig. 3B). In contrast, the h1h2 loop of BCMA was not found to be important for ligand binding (15), while this loop is essentially absent in BR3 (23). Gly^{94} and His^{96} might play a role in stabilizing the structure given that

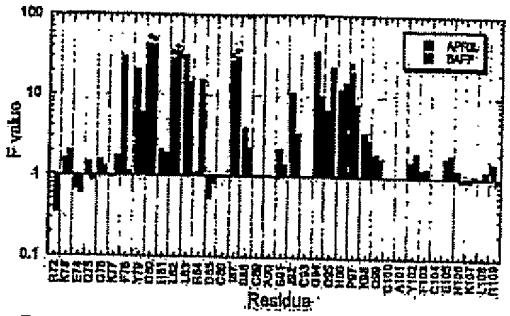

FIG. 4. Shotgun alanine scanning mutagenesis of TACI_d2 binding to BAFF or APRIL. The normalized frequency ratios (*F*) observed for each of the scanned positions in TACI_d2 obtained from sequences of positive clones after two rounds of selection for binding to APRIL (*hatched*) or BAFF (*solid*) are plotted. Those *bars* with an *asterisk* (*) above indicate values that represent a lower limit because Ala was not observed at these positions.

the glycine adopts a positive phi value (which would not be readily accommodated by alanine), and His^{96} is buried in the TACI_d2 structure, thus loss of binding upon alanine substitution of these residues might be the result of indirect effects. However, Gln^{95} and Pro^{97} line the concave surface of TACI_d2 and could contribute directly to ligand binding (see below). Finally, several positions showed different effects on APRIL and BAFF binding and are likely to be involved in ligand specificity. For example, Phe^{78} was found to be important only for APRIL binding (*F* = 29 for APRIL and 1.1 for BAFF), whereas mutation of Arg^{84} only showed losses on BAFF binding (*F* = 1.1 for APRIL and 16 for BAFF).

Structure of APRIL Bound to TACI_d2—The crystal structure of APRIL in complex with TACI_d2 was determined at 1.9 Å resolution by molecular replacement and refined to an R/R_{free} of 16.7/20.3%, respectively (Fig. 5, Table S4). The structure of the APRIL component of the complex is very similar to the structure of free APRIL, except that several loops (AA', CD, and EF) are ordered in the complex, which were either disordered or only marginally ordered in structures of free APRIL (28). The bound structure of TACI_d2 is similar to the NMR structure (backbone r.m.s.d. of the three chains in the asymmetric unit to the mean NMR structure is 0.74 ± 0.06 for residues 76–104). However, the h2 helix is longer in two of the crystallographic chains (Fig. 3A).

In general terms, TACI_d2 binds APRIL in a manner similar to the way the homologous receptor, BCMA, binds BAFF (26). The DXL motif forms a hydrophobic ridge with the two leucine residues (82 and 83) at the tip of the DXL turn nestled in a hydrophobic pocket on APRIL that is ringed by APRIL residues Phe^{187}, Val^{172}, Arg^{188}, Ile^{183}, Tyr^{199}, and Arg^{222} (Fig. 5B). The backbone of residues forming this pocket shows only modest changes from the structure of APRIL alone. In contrast, the side chains (Phe^{187}, Thr^{158}, Arg^{156}, Tyr^{199}, and Arg^{222}), which form the "rim" of the pocket, are more ordered in the complex. The first helix of TACI, h1, contacts APRIL residues 194–197 in the EF loop. The receptor h1h2 loop contacts four loops on APRIL (EF, CD, GH, and AA').

The APRIL binding surface on TACI_d2 encompasses the entire concave surface defined by mutagenesis; ~1,700 $Å^2$ are buried in this extensive interface (Fig. 6A). The functionally important residues, Leu^{82}, Leu^{83}, and Ile^{87} in the DXL hairpin, Ile^{92} in h1, and Gln^{95} and Pro^{97} in the h1h2 loop, form a predominantly hydrophobic surface that interacts with APRIL. Only Asp^{80} in the DXL motif and Gln^{95} in the h1h2 loop participate in hydrogen bonds. The backbone carbonyl of Gln^{95}

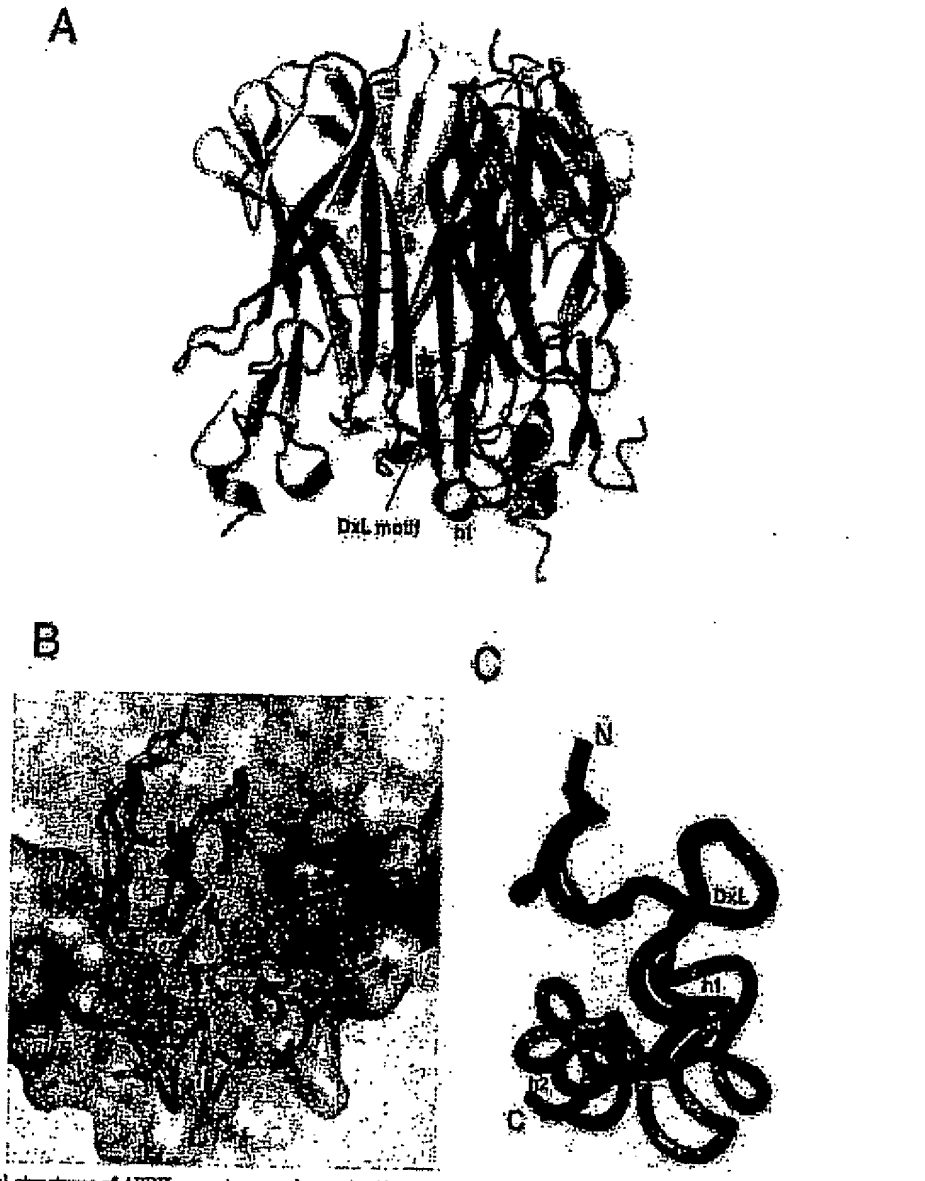

FIG. 6. Crystal structures of APRIL-receptor complexes. *A*, ribbon structure of APRIL/TACI_d2 complex. The APRIL trimer (residues 105–241) is shown in *gray*, *yellow*, and *pink*, and the three copies of TACI_d2 are colored *blue*. In this orientation, the membrane of the TACI-presenting cell would be located at the bottom of the figure. *B*, comparison of APRIL-receptor complexes. The DXL motif, h1 and the h1h2 loop, are shown for both TACI_d2 (*blue*) and BCMA (*yellow*, labels *underlined*). Side chains from APRIL (*white*, labels *italicized*) which interact with receptor are rendered as *sticks*. *C*, comparison of TACI_d2, BCMA, and BR3. Ribbon drawings of the three receptors for APRIL and/or BAFF are shown superimposed using the backbone atoms of residues in the DXL motif (residues 79–85, 14–20, and 25–31 in TACI_d2, BCMA, and BR3, respectively). The TACI_d2 (*blue*) and BCMA (*yellow*) structures are taken from the crystal structures of their respective APRIL-receptor complex, whereas the BR3 (*green*) structure is from the crystal structure of the BAFF·BR3 complex, 1OQE (26).

forms a hydrogen bond to the backbone amide of Phe^{187}, whereas the side chain carbonyl forms hydrogen bonds to the guanidinium moiety of $Arg^{197'}$ in the EF loop from an adjacent protomer (Fig. 5*B*). Furthermore, the side chain amide group of Gln^{93} forms hydrogen bonds to the carbonyls of Thr^{182} in the APRIL CD loop and Met^{191} in the EF loop. This network of hydrogen bonds likely contributes to stabilizing the conformation of the APRIL CD and EF loops, which are poorly ordered in the absence of receptor. Neither receptor residue Tyr^{79} nor His^{86} interacts directly with APRIL, hence both are likely important for binding because of indirect effects on protein stability. In contrast, Phe^{78} probably has both structural and

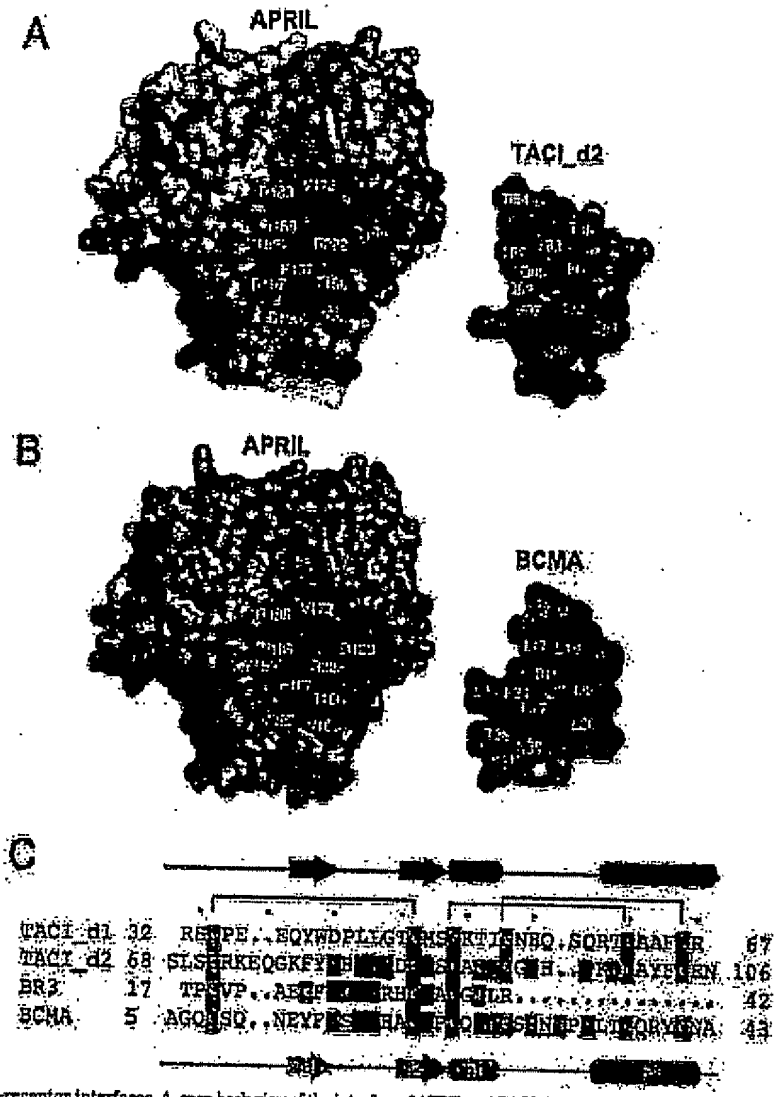

FIG. 6. APRIL-receptor interfaces. *A*, open book view of the interface of APRIL and TACI_d2. APRIL and one copy of TACI_d2 are rendered as molecular surfaces. Residues in the interface are colored by percent of accessible surface area buried upon complex formation (25–49%, *yellow*; 50–74%, *orange*; 75–100%, *red*). *B*, open book view of the interface of APRIL and BCMA. APRIL and one copy of BCMA are rendered as molecular surfaces. Residues in the interface are colored by percent of accessible surface area buried upon complex formation as in *A*. *C*, sequence alignment of TACI, BR3, and BCMA CRDs. Secondary structural elements of TACI_d2 and BCMA when bound to APRIL are indicated above and below their respective sequences. Cysteine residues are highlighted in *orange* and their connectivity in TACI and BCMA is shown above the alignment. The cysteine connectivity in TACI_d1 is expected to be the same as in TACI_d2. Receptor residues that have *F* values >6 in shotgun alanine scanning for APRIL binding (TACI_d2, BCMA) and BAFF binding (BR3) are colored *red*. TACI_d2, BCMA, and BR3 residues that bury >50% accessible surface area on binding APRIL (TACI_d2, BCMA), or BAFF (BR3) are shaded *gray*. BCMA residues that bury >50% accessible surface area in binding BAFF are *underlined* (25). Every fifth TACI_d2 residue is marked by a *dot* above the alignment.

functional roles: it does not bury significant surface area (3 Å^2) but helps position Phe^{167} of APRIL, as well as restricts the relative orientation of the two submodules of TACI_d2.

Structure of APRIL Bound to BCMA—Despite the fact that TACI encodes two CRDs, the structural and functional results discussed above argue that ligand binding by TACI can be accounted for by a single domain akin to that of the single CRD-containing receptor BCMA. Hence, to compare directly the interactions provided by TACI_d2 with those from BCMA, we determined the structure of the APRIL/BCMA complex to 2.35 Å resolution with an R/R_{free} of 17.8/21.3% (Fig. 5 and Table S4). The structure of the APRIL trimer is identical in the two complexes with the exception of a few solvent exposed residues. The secondary structural elements of BCMA are similar to those in TACI_d2, but the relative orientation of the helices with respect to the DXL hairpin differs and results in significantly different surfaces being presented to the ligand (Figs. 5 and 6).

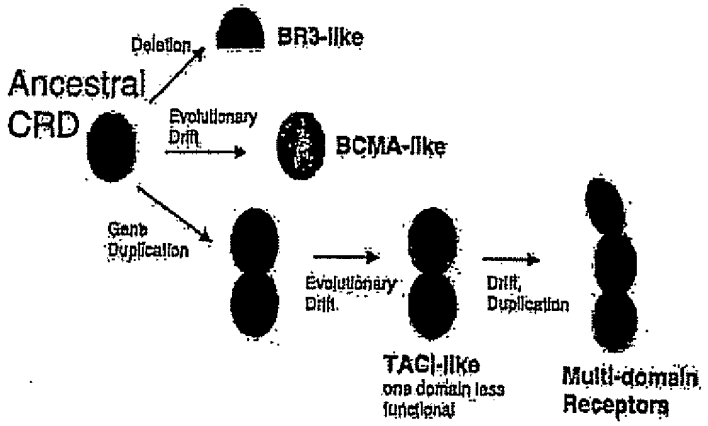

FIG. 7. Evolution of the TNFR superfamily. Sketch of the possible steps in the evolution of BR3-like, BCMA-like, and multidomain TNFR-like receptors from an ancestral single domain receptor. TACI-like receptors with two CRDs, one of which is less functional, may represent a crucial step between single-domain and specialized multidomain receptors.

The structure of BCMA and its ligand binding mode in this APRIL complex is similar to that in the BAFF complex reported previously (26), with the exception of the h1h2 loop. The r.m.s.d. between BCMA in the two complexes is 0.8 Å overall, 0.6 Å if residues 29–34 are excluded. In the APRIL·BCMA structure, BCMA residues 29–34 make more extensive interactions with the GH and AA′ loops of APRIL than does BCMA with the corresponding parts of BAFF in the BAFF·BCMA complex.

BCMA binds APRIL with significantly higher affinity than it binds BAFF and buries more surface area when bound to APRIL (1,600 Å^2) than when bound to BAFF (1,300 Å^2) (Fig. 6*B*). The extra buried surface area is contributed by both the ligand and the receptor. From the receptor, Leu^{28}, and residues 31–38 all contribute significantly more surface area in complex with APRIL than when bound to BAFF. These residues contact areas of APRIL which are different in both sequence and conformation from the corresponding regions in BAFF including the tip of the AA′ loop (residues 120–123) and the EF loop (residues 194–199) where there is a 2-residue insertion in APRIL with respect to BAFF.

DISCUSSION

The Membrane-proximal CRD Is the High Affinity Ligand Binding Domain of TACI—We have shown that the second CRD of TACI (TACI_d2) binds both APRIL and BAFF with high affinity, whereas the first CRD does not. Furthermore, binding to either ligand is not enhanced by the addition of the first CRD, as would be present in the extracellular domain of the full-length gene product. Consistent with the membrane-proximal CRD2 being the primary determinant for ligand binding, we found that an alternatively spliced form of TACI, shortTACI, which lacks CRD1, can induce both APRIL- and BAFF-dependent NFκB activation in transfected cells. Given this, TACI seems to share more similarity in its ligand binding properties to the more unusual members of the TNFR family, BCMA and BR3, than to the multidomain TNF receptors such as TNFR1 or DR5.

Similarities and Differences among the Receptors for APRIL and BAFF—A superposition of TACI_d2, BCMA, and BR3 reveals remarkable similarity in the structure of the DXL hairpin in the N-terminal submodule of the domain (Fig. 5*C*). Significant differences are apparent, however, in the C-terminal submodule; the secondary structural elements in this region (h1, loop, and h2) have different relative orientations in TACI_d2 and BCMA and, with the exception of h1, are missing in BR3. For example, although the TACI_d2 and BCMA hairpins superimpose well, with a backbone r.m.s.d. of 0.31 Å^2 (residues 77–88 and 12–23, respectively), the overall backbone r.m.s.d. for the domain is 1.5 Å. Importantly, these differences appear to be a property of the different receptors themselves and not a product of a ligand-induced conformational change given that the solution structure of free TACI_d2 and the crystal structure of TACI_d2 in complex with APRIL are essentially the same in this region (Fig. 3*A*), as are the structures of BCMA in complex with BAFF or APRIL. Such differences in domain structure indicate that although all three receptors can interact with their respective ligands in a similar fashion through their DXL motifs, the interactions through their C-terminal submodules will differ and likely will dictate the relative affinity and specificity among ligand-receptor pairs within the APRIL/BAFF family. For example, Arg^{27} from BCMA packs against the same region of APRIL as Pro^{87} from TACI_d2, despite the fact that they are offset in a primary sequence alignment by 5 residues (Figs. 5*B* and 6*C*). Furthermore, Gln^{93} in TACI_d2 makes extensive contacts with APRIL and yet has no counterpart in BCMA.

APRIL-Receptor Complexes Compared with BAFF·BR3—The APRIL-receptor interfaces, although similar to BAFF·BR3, make significant contacts beyond those mediated through the DXL motif. In BAFF·BR3, the DXL hairpin makes the majority of receptor contacts (~75% of the buried surface area contributed by the receptor) (24, 26); whereas in both the APRIL·TACI and APRIL·BCMA complexes, the receptor DXL hairpin contributes only ~50% of the total buried surface area. Docking BR3 onto APRIL shows that the BR3 hairpin could be accommodated readily with no steric clashes and result in an interface of ~1,000 Å^2 (~80% from the DXL hairpin), yet BR3 does not bind APRIL. Instead, APRIL seems to require additional contacts from other portions of the receptor to form high affinity interactions. The partial CRD of BR3 does not contain the second submodule and hence cannot provide these contacts. Furthermore, one of the key APRIL-specific binding determinants (Phe^{78} of TACI; Tyr^{13} of BCMA) identified by alanine scanning is not conserved in BR3 (Fig. 6*C*).

An Extensive Ligand Binding Interface Presented By a Single Receptor CRD—TACI_d2 differs from multidomain TNFRs by using most of its CRD surface to contact ligand. (Fig. 6*A*). In the case of TNFR1 and DR5 in complex with their respective ligands, the majority of the ligand binding interactions stem from one loop from each of two adjacent CRDs (analogous to the hairpin in BAFF and APRIL receptors, although differing in length and conformation), and both CRDs are required for

ligand binding (44–47). BR3 does not deviate from this approach in that contacts are made primarily from a single receptor loop, except that it manages to generate high affinity BAFF binding through interactions with one receptor domain. However, TACI_d2 binds APRIL using a continuous surface formed by residues from every secondary structural element in the domain. In so doing, the APRIL-TACI_d2 interface (1,700 Å^2) ends up being similar in overall size to the multidomain TNFR binding sites (*e.g.* lymphotoxin-TNFR1 buries ~2,100 Å^2) yet only occupies a focused region on the ligand surface.

Model of Intact TACI_d1d2—A homology model of TACI_d1 was generated based on the structure of TACI_d2. Human TACI_d1 is predicted to adopt a similar DXL hairpin fold that could bind ligand in a fashion similar to that seen for the other APRIL or BAFF receptors. TACI_d1 is also predicted to share the same disulfide connectivity and helical secondary structure for its C-terminal submodule. However, the h1h2 loop, which makes key contacts with ligand in the APRIL/TACI_d2 complex, differs in length and amino acid sequence between TACI domains (Fig. 6*C*). Thus, these changes are likely to be responsible for the lower affinity of TACI_d1 for ligand binding.

Using this model of TACI_d1, a model of intact TACI_d1d2 was constructed. The connectim between the two CRDs in TACI consists of four residues. This is different from other multidomain TNFR where typically there are only 1–2 residues between the last cysteine of a CRD and the first cysteine in the following CRD, with these residues forming part of a β-strand. The connection in TACI is unlikely to form a β-strand because the final cysteine of CRD1 is expected to be part of a small helix, similar to that of TACI_d2 or BCMA. With uncertainty in the conformation of the connecting linker, the relative orientation of the two CRDs with respect to each other is difficult to predict. One could model CRD1 such that it touches the ligand surface while CRD2 occupies the primary receptor binding site. However, because the addition of CRD1 adds no further binding energy compared with that of CRD2 alone, CRD1 does not likely make extensive contacts to ligand.

Despite the uncertainty in the orientation of TACI_d1 with respect to TACI_d2, some models of possible interactions of two-domain TACI with ligand can be ruled out on the basis of steric considerations. Docking the two-domain construct of TACI to BAFF (PDB code 1OQD) (30) indicates that the hypothesis raised by Kim and co-workers (24) that TACI might bridge two binding sites on adjacent trimers in the higher order virus-like BAFF oligomer is physically impossible. In order for CRDs 1 and 2 to bind DXL pockets on adjacent BAFF trimers simultaneously, the final CRD1 cysteine (Cys^{55}) would need to be ~30 Å from the first cysteine (Cys^{71}) in CRD2, which is farther than can be spanned by the 4-residue (^{67}RSLS^{70}) interdomain linker. Similarly, TACI CRDs 1 and 2 cannot simultaneously bind in the same manner to two different APRIL (or BAFF) protomers within the same trimer as the distance between the C-terminal cysteine of CRD1 to the N-terminal cysteine of CRD2 would need to be ~40 Å^2 to reach the two binding pockets.

TACI: An Intermediate in the Evolution of the Multidomain TNFR Superfamily?—Despite the presence of two CRDs in the human TACI sequence, TACI appears to function like a single domain receptor requiring only CRD2 for high affinity interactions with either of its ligands. The presence of two domains, each with a DXL motif, is likely the result of a gene duplication event that added a second copy to an original DXL-containing single-domain receptor. In this scenario, the additional domain is not functionally required for ligand binding, thus random mutations could accumulate in CRD1 over time such that it no longer can bind tightly to either APRIL or BAFF. In this context, CRD1 would be considered an evolutionary remnant. Consistent with this hypothesis, the DXL motif is not conserved in murine TACI CRD1. Thus, TACI might recapitulate an early event in the evolution of the TNFR superfamily, the transition from one domain to many (Fig. 7). In an intermediate step, represented by TACI, the extra domain(s) are only partially functional having not yet evolved to recognize different sites on the ligand (although the formal possibility remains that TACI CRD1 could play another, as yet undefined, role). In other TNFR family members, extra domains have been optimized to function together to form the high affinity complex. Additional CRDs can have roles in providing stability, regulation (42), or in forming further contacts to the ligand to optimize affinity and specificity. Thus in the structures of the receptors for APRIL and BAFF, two opposing evolutionary options are represented: BR3 showing the minimization of a canonical CRD to an even more compact format and TACI showing a possible intermediate in the evolution of larger, more complex, multidomain proteins.

Acknowledgments—We thank Deanne Compean for initial crystallization trials of the APRIL-receptor complexes and help with x-ray data collection; Wayne Fairbrother for helpful discussions; and members of the DNA synthesis, DNA sequencing, N-terminal sequencing, and mass spectrometry groups at Genentech. The use of APS beamline 19BM was supported by the United States Department of Energy, Office of Energy Research, under Contract W-31-109-ENG-38.

REFERENCES

1. Locksley, R. M., Killeen, N., and Lenardo, M. J. (2001) *Cell* 104, 487–501
2. Hahne, M., Kataoka, T., Schröter, M., Hofmann, K., Irmler, M., Bodmer, J.-L., Schneider, P., Bernard, T., Holler, N., French, L. E., Sordat, B., Rimoldi, D., and Tschopp, J. (1998) *J. Exp. Med.* 188, 1185–1190
3. Medema, J. P., Pinedlas-Canuas, L., Hardenbark, G., and Hahne, M. (2003) *Cell Death Differ.* 10, 1121–1125
4. Schneider, P., MacKay, F., Steiner, V., Hofmann, K., Bodmer, J.-L., Holler, N., Ambrose, C., Lawton, P., Bixler, S., Acha-Orbea, H., Valmori, D., Romero, P., Werner-Favre, C., Zahler, R. H., Browning, J. L., and Tschopp, J. (1999) *J. Exp. Med.* 189, 1747–1756
5. Moore, P. A., Belvedere, O., Orr, A., Pieri, K., LaFleur, D. W., Feng, P., Soppet, D., Charters, M., Gentz, R., Parmelee, D., Li, Y., Galperina, O., Giri, J., Roschke, V., Nardelli, B., Carrell, J., Sosnovtseva, S., Greenfield, W., Ruben, S. M., Olsen, H. S., Fikes, J., and Hilbert, D. M. (1999) *Science* 285, 260–263
6. Schneemann, B., Gunnermann, J. L., Vera, K., Cachero, T. G., Shulga-Morskaya, S., Dobles, M., Frew, R., and Scott, M. L. (2001) *Science* 293, 2111–2114
7. Thompson, J. S., Bixler, S. A., Qian, F., Vora, K., Scott, M. L., Cachero, T. G., Hession, C., Schneider, P., Sizing, I. D., Mullen, C., Strauch, K., Zafari, M., Benjamin, C. D., Tschopp, J., Browning, J. L., and Ambrose, C. (2001) *Science* 293, 2108–2111
8. Yan, M., Brady, J. R., Chan, B., Lee, W. P., Hsu, B., Harless, S., Cancro, M., Grewal, I. S., and Dixit, V. M. (2001) *Curr. Biol.* 11, 1547–1552
9. Mackay, F., Schneider, P., Rennert, P., and Browning, J. (2003) *Annu. Rev. Immunol.* 21, 231–264
10. Marsters, S. A., Yan, M., Pitti, R. M., Haas, P., Dixit, V. M., and Ashkenazi, A. (2001) *Curr. Biol.* 10, 785–788
11. Rennert, P., Schneider, P., Cachero, T. G., Thompson, J., Trabach, L., Hertig, S., Holler, N., Qian, F., Mullen, C., Strauch, K., Browning, J. L., Ambrose, C., and Tschopp, J. (2000) *J. Exp. Med.* 192, 1677–1684
12. Thompson, J. S., Schneider, P., Kalled, S. L., Wang, L., Lefevre, E. A., Cachero, T. G., MacKay, F., Bixler, S. A., Zafari, M., Liu, Z.-Y., Woodcock, S. A., Qian, F., Batten, M., Madry, C., Richard, Y., Benjamin, C. D., Browning, J. L., Tsapis, A., Tschopp, J., and Ambrose, C. (2000) *J. Exp. Med.* 192, 129–135
13. Wu, Y., Bressette, D., Carrell, J. A., Kaufman, T., Feng, P., Taylor, K., Gan, Y., Cho, Y. H., Garcia, A. D., Gollatz, E., Dimke, D., LaFleur, D., Migone, T. S., Nardelli, B., Wei, P., Ruben, S. M., Ullrich, S. J., Olsen, H. S., Hanakawa, P., Moore, P. A., and Baker, K. P. (2000) *J. Biol. Chem.* 275, 35478–35485
14. Pelletier, M., Thompson, J. S., Qian, F., Bixler, S. A., Gong, D., Cachero, T., Gilbride, K., Day, E., Zafari, M., Benjamin, C., Gorelik, L., Whitty, A., Kalled, S. L., Ambrose, C., and Hsu, Y.-M. (2003) *J. Biol. Chem.* 278, 33127–33133
15. Patel, D. R., Wallweber, H. J. A., Yin, J., Shriver, S. K., Marsters, S. A., Gordon, N. C., Starovasnik, M. A., and Kelley, R. F. (2004) *J. Biol. Chem.* 279, 18727–18735
16. Yan, M., Wang, H., Chan, B., Roose-Girma, M., Erickson, S., Baker, T., Tumas, D., Grewal, I. S., and Dixit, V. M. (2001) *Nat. Immunol.* 2, 638–643
17. Seshasayee, D., Valdez, P., Yan, M., Dixit, V. M., Tumas, D., and Grewal, I. S. (2003) *Immunity* 18, 279–288
18. O'Connor, B. P., Raman, V. S., Erickson, L. D., Cook, W. J., Weaver, L. K., Ahonen, C., Lin, L.-L., Mantchev, G. T., Bram, R. J., and Noelle, R. J. (2004) *J. Exp. Med.* 199, 91–97
19. Bodmer, J.-L., Schneider, P., and Tschopp, J. (2002) *Trends Biochem. Sci.* 27, 19–26
20. von Bülow, G.-U., and Bram, R. J. (1997) *Science* 278, 138–141

21. Wiley, S. R., Cassiano, L., Lofton, T., Davis-Smith, T., Winkles, J. A., Lindner, V., Liu, H., Daniel, T. O., Smith, C. A., and Fanslow, W. C. (2001) *Immunity* 15, 837–845
22. Kappler, S., Manly, W. S., Chen, P., Tumar, R. S., Eby, M. T., Chapo, J., Chew, S., Rathore, N., Zachariah, S., Sinha, S. K., Abrams, J. M., and Chaudhary, P. M. (2003) *Oncogene* 22, 4850–4857
23. Gordon, N. C., Pan, B., Hymowitz, S. G., Yin, J., Kelley, R. F., Cochran, A. G., Yan, M., Dixit, V. M., Fairbrother, W. J., and Starovasnik, M. A. (2003) *Biochemistry* 42, 5977–5983
24. Kim, H. M., Yu, K. S., Lee, M. E., Shin, D. R., Kim, Y. S., Park, S.-G., Yoo, O. J., Lee, H., and Lee, J.-O. (2003) *Nat. Struct. Biol.* 10, 342–348
25. Kayagaki, N., Yan, M., Seshasayee, D., Wang, H., Lee, W., French, D. M., Grewal, I. S., Cochran, A. G., Gordon, N. C., Yin, J., Starovasnik, M. A., and Dixit, V. M. (2002) *Immunity* 17, 515–524
26. Liu, Y., Hong, X., Kappler, J., Jiang, L., Zhang, R., Xu, L., Pan, C.-H., Martin, W. E., Murphy, R. C., Shu, H.-B., Dai, S., and Zhang, G. (2003) *Nature* 423, 49–56
27. Zhang, G. (2004) *Curr. Opin. Struct. Biol.* 14, 154–160
28. Wallweber, H. J. A., Compaan, D. M., Starovasnik, M. A., and Hymowitz, S. G. (2004) *J. Mol. Biol.* 343, 283–290
29. Hariputra, M., Cachero, T. G., Qian, F., Bortsick-Sjodin, A., Mullen, C., Strauch, K., Hsu, Y.-M., and Halled, S. L. (2002) *J. Mol. Biol.* 315, 1145–1154
30. Liu, Y., Xu, L., Opalka, N., Kappler, J., Shu, H.-B., and Zhang, G. (2002) *Cell* 108, 383–394
31. Oren, D. A., Li, Y., Volovik, Y., Morris, T. S., Dhavia, C., Das, K., Galperina, O., Gaetz, R., and Arnold, E. (2002) *Nat. Struct. Biol.* 9, 288–292
32. Weiss, G. A., Watanabe, C. K., Zhong, A., Goddard, A., and Sidhu, S. S. (2000) *Proc. Natl. Acad. Sci. U. S. A.* 97, 8950–8954
33. Skelton, N. J., Koehler, M. F. T., Zobel, K., Wong, W. L., Yeh, S., Pisabarro, M. T., Yin, J., Lasky, L. A., and Sidhu, S. S. (2003) *J. Biol. Chem.* 278, 7645–7654
34. Cavanagh, J., Fairbrother, W. J., Palmer, A. G., III, and Skelton, N. J. (1996) *Protein NMR Spectroscopy: Principles and Practice*, Academic Press, San Diego
35. Neri, D., Szyperski, T., Otting, G., Senn, H., and Wüthrich, K. (1989) *Biochemistry* 28, 7510–7516
36. Skelton, N. J., Akke, M., Kördel, J., Palmer, A. G. P., Rance, M., and Chazin, W. J. (1993) *J. Magn. Reson. 102*, 253–264
37. Herrmann, T., Güntert, P., and Wüthrich, K. (2002) *J. Mol. Biol.* 319, 209–227
38. Cornilescu, G., Delaglio, F., and Bax, A. (1999) *J. Biomol. NMR* 13, 289–302
39. Otwinowski, Z., and Minor, W. (1997) *Methods Enzymol.* 276, 307–326
40. Collaborative Computational Project 4 (1994) *Acta Crystallogr. Sect. D Biol. Crystallogr.* 50, 760–763
41. Yan, M., Marsters, S. A., Grewal, I. S., Wang, H., Ashkenazi, A., and Dixit, V. M. (2000) *Nat. Immunol.* 1, 37–41
42. Chan, F. K.-M., Chun, H. J., Zheng, L., Siegel, R. M., Bui, K. L., and Lenardo, M. J. (2000) *Science* 288, 2351–2354
43. Cochran, A. G., Tong, R. Y., Starovasnik, M. A., Park, E. J., McDowell, R. S., Theaker, J. E., and Skelton, N. J. (2001) *J. Am. Chem. Soc.* 123, 625–632
44. Hymowitz, S. G., Christinger, H. W., Fuh, G., Ultsch, M., O'Connell, M., Kelley, R. F., Ashkenazi, A., and de Vos, A. M. (1999) *Mol. Cell* 4, 563–571
45. Banner, D. W., D'Arcy, A., Janes, W., Gentz, R., Schoenfeld, H.-J., Broger, C., Loetscher, H., and Lesslauer, W. (1993) *Cell* 73, 431–445
46. Cha, S.-S., Sung, B.-J., Kim, Y.-A., Song, Y.-L., Kim, H.-J., Kim, S., Lee, M.-S., and Oh, B.-H. (2000) *J. Biol. Chem.* 275, 31171–31177
47. Mongkolsapaya, J., Grimes, J. M., Chen, N., Xu, X.-N., Stuart, D. I., Jones, E. Y., and Screaton, G. R. (1999) *Nat. Struct. Biol.* 6, 1048–1053

SUPPLEMENTARY MATERIAL

Table S1. NMR experiments used to characterize the solution structure of TACI_d2

Experiment	SF (MHz)	Dim.	Nuc.	NS	SW (Hz)	Points (complex)	τ_m (ms)	Offset (ppm)
^{1}H-^{15}N HSQC	600	1	N	4	1275.5	256*		118.0
		2	HN		8620	4096*		4.92
^{1}H-^{13}C HSQC	500	1	C	4	4032	512*		32.4
		2	H		6250	2048*		4.86
TOCSY-HSQC	600	1	H	16	6024	128*	69	4.92
		2	N		1275.5	32*		118.0
		3	HN		8620	1024*		4.92
NOESY-HSQC	600	1	H	16	6024	128*	200	4.92
		2	N		1275.5	32*		118.0
		3	HN		8620	1024*		4.92
HNHB	600	1	HB	32	5760	90*		4.92
		2	N		1275.5	32*		118.0
		3	HN		8620	1024*		4.92
CBCA(CO)NH	600	1	CAB	16	9058	29*		44.4
		2	N		1340	30*		119.3
		3	HN		6250	1024*		4.93
HCCH-TOCSY	600	1	H	8	4202	128*	25	4.93
		2	C		4854	42*		32.9
		3	H		6250	2048*		4.93
^{13}C-edited NOESY	600	1	H	16	5768	128*	50, 150	4,93
		2	C		4930	32*		32.9
		3	H		6250	1024*		4.93
^{1}H-^{1}H NOESY	600	1	H	96	5763	400*	200	4,93
		2	H		6250	4096*		4.93
{^{1}H}-^{15}N NOE	500	1	H	16	6510	2048*		4.92
		2	N		1014.2	128*		119.3

Table S2. Statistics for the Solution Structure of TACI_d2

Parameter	Ensemble
Input restraints	
NOE Total	466;
Intra-residue; Sequential; Medium-range; Long-range	124; 95; 123; 124
Dihedral Angles Total	188
ϕ; ψ; ω^a; $\chi_1{}^b$; $\chi_3{}^c$	40; 27; 90; 25; 6
Violations	
RMSD from experimental restraints	
NOE-distance (Å)	0.0045 ± .0009
Dihedral (°)	0.18 ± 0.04
NOE distance violations	
Number > 0.01 Å; > 0.1 Å	12.4 ± 2.4; 0.0
Mean maximum violations (Å)	0.04 ± 0.01
Dihedral violations	
Number > 0.1°	7.8 ± 2.3
Mean maximum violations (°)	0.72 ± 0.24
RMSD from idealized geometry	
Bonds (Å)	0.0009 ± 0.0001
Angles (°)	0.27 ± 0.01
Impropers (°)	0.12 ± 0.01
Energies	
Energy components (kcal.mol.$^{-1}$)	
NOE (466)	0.36 ± 0.12
CDIH (188)	0.09 ± 0.06
Bonds	0.70 ± 0.18
Angles	15.34 ± 0.96
Impropers	0.88 ± 0.15
Vanb der Waal's	8.06 ± 1.74
Stereochemistry	
Ramachandran (%)	
Favored; Allowed; Generous; Disallowed	66.8; 31.6; 1.6; 0

Structural precision	
Mean RMSD to mean structure (Å)	
Backbone	
Residues 76-104	0.55 ± 0.08
Residues 76-88	0.28 ± 0.05
Residues 89-104	0.25 ± 0.10
Heavy	
Residues 76-104	0.92 ± 0.10
Residues 76-88	0.81 ± 0.13
Residues 89-104	0.61 ± 0.10

[a] Amide groups were restained to be within 10° of planarity. [b] Chi-1 angles were restrained to a particular staggered rotamer ± 30°. [c] In the case of cysteine residues for which a unique rotamer could not be defined by the HNHB and NOE data, two or three overlapping restraints were applied to limit the side chain to occupy staggered conformations only. Chi-3 angle restraints were restrained to ±90 ± 20° by using two overlapping dihedral angle restraints.

Table S3: Combinatorial Shotgun Alanine Scan of TACI_d2

		BAFF selection				APRIL selection				Display selection				*F* (BAFF)			*F* (APRIL)		
residue	m2,m3	wt	Ala	m2	m3	wt	Ala	m2	m3	wt	Ala	m2	m3	Ala	m2	m3	Ala	m2	m3
R72	G, P	14	20	24	12	21	10	25	15	18	9	12	9	0.4	0.4	0.6	1.1	0.6	0.7
K73	E, T	23	20	18	9	20	22	15	14	4	7	23	14	2.0	7.3	8.9	1.6	7.7	5.0
E74		38	31			41	30			32	16			0.6			0.7		
Q75	E, P	17	14	21	18	20	10	25	16	14	10	12	12	0.9	0.7	0.8	1.4	0.7	1.1
G76		42	28			46	25			26	22			1.3			1.6		
K77	E, T	19	12	21	18	19	21	14	17	13	14	13	8	1.7	0.9	0.6	1.0	1.4	0.7
F78	S, V	29	12	6	23	62	1	0	8	15	7	16	10	1.1	5.2	0.8	29	>66	5.2
Y79	D, S	45	4	0	0	39	0	0	1	19	10	4	15	5.9	>9.5	>36	>21	>8.2	31
D80		70	0			71	0			30	18			>42			>43		
H81	D, P	25	7	8	49	23	6	11	24	19	10	8	30	1.9	1.3	0.8	2.0	0.9	1.5
L82	P, V	50	0	0	0	40	0	0	0	14	10	17	7	>36	>61	>25	>29	>49	>20
L83	P, V	41	3	1	25	57	2	0	12	14	15	5	14	15	15	1.6	31	>20	4.8
R84	G, P	45	2	3	0	19	12	9	0	13	9	11	15	16	13	>52	1.1	1.8	>22
D85		32	37			26	45			25	23			0.8			0.5		
C86																			
I87	T, V	28	0	0	22	25	0	0	15	13	14	10	11	>30	>22	1.1	>27	>19	1.4
S88		35	15			32	8			24	23			2.2			3.8		
C89																			
A90																			
S91		33	17			30	10			28	20			1.4			2.1		
I92	T, V	12	3	9	26	26	2	3	9	13	11	9	15	3.4	0.9	0.5	11	6.0	3.3
C93																			
G94		46	4			39	1			25	22			10			34		
Q95	E, P	46	2	1	0	33	5	2	0	11	11	13	13	23	58	>54	6.6	21	>39
H96	D, P	44	3	0	3	36	3	0	1	12	12	8	16	15	>29	20	12	>24	48
P97		47	3			40	0			32	16			7.8			>20		
K98	E, T	31	13	1	5	23	8	4	5	10	12	12	14	2.9	37	8.7	3.5	6.9	6.4
Q99	E, P	14	9	17	13	23	8	8	15	14	15	13	23	1.7	0.8	1.8	1.9	1.6	1.5
C100																			
A101																			
Y102	D, S	9	7	12	25	12	9	9	24	9	14	7	35	2.0	0.6	1.4	1.6	0.8	1.5
F103	S, V	23	7	8	15	26	7	4	17	23	9	23	10	1.3	2.9	0.7	1.3	5.8	0.6
C104																			
E105		30	23			29	25			22	43			1.9			1.7		
N106	D, T	6	23	12	12	13	17	15	9	12	21	18	14	0.9	1.5	1.2	1.2	1.2	1.6
K107	E, T	10	20	8	15	8	24	7	14	12	22	15	16	1.1	1.9	1.1	0.9	2.1	1.1
L108	P, V	15	9	17	12	10	11	18	15	15	11	25	14	1.2	1.5	1.2	1.0	1.4	0.9
R109	G, P	8	10	16	19	12	6	16	20	14	9	19	23	0.9	1.2	1.2	1.5	1.2	1.2

The occurrence of the wild-type residue (wt) or each mutation (Ala, m2, m3) found among sequenced clones following two rounds of binding by ligand selection (BAFF or APRIL) or

display selection (anti-tag) is shown for the scanned positions in TACI_d2. The occurrence of wild-type divided by mutant provides a wt/mutant ratio for each position (not shown). A normalized frequency ratio (F) was calculated to quantify the effect of each mutation on ligand-binding while accounting for display efficiencies: i.e. F = [wt/mutant (ligand selection)]÷ [(wt/mutant (display selection)]. Deleterious mutations have ratios >1, while advantageous mutations have ratios <1; boldface values indicate a >10-fold effect and are considered significant. Certain F values represent a lower limit since Ala, m2, or m3 were not observed at these sites in ligand selection.

Table S4. Data Collection and Refinement Statistics For APRIL–Receptor Complexes

	APRIL–TACI_d2	APRIL–BCMA
Data Collection		
Space Group	$P2_12_12_1$	$P6_1$
Resolution (Å)	50–1.90 (1.97-1.90)[a]	50-2.35 (2.43-2.35)[a]
Unit cell constants (Å)	$a = 59.3$ $b = 91.8$ $c = 102.3$	$a = 114.3$ $c = 91.2$
R_{sym}[b]	0.086 (0.347)[a]	0.067 (0.425)[a]
No. observations	289,762	266,614
Unique reflections	44,579	28,292
Completeness (%)	99.6 (100)[a]	99.9 (100)[a]
Asymmetric Unit	1 APRIL trimer; 3 TACI_d2	1 APRIL trimer; 3 BCMA
Refinement		
Resolution (Å)	30-1.90	30-2.35
Final R[c], R_{free} (%)	16.7, 20.3	17.8/21.3%
No. solvent atoms	131	37
Rmsd bonds (Å)	0.009	0.010
Rmsd angles (°)	1.2	1.2
Rmsd bonded Bs ($Å^2$)	3.0	2.8
Ramachandran Plot (%)[d]	92.3; 7.7; 0; 0	91.5; 8.3; 0.2; 0

[a] Numbers in parentheses refer to the highest resolution shell.

[b] $R_{sym} = \Sigma |I - \langle I \rangle| / \Sigma I \langle I \rangle$ is the average intensity of symmetry related observations of a unique reflection.

[c] $R = \Sigma |F_o - F_c| / \Sigma F_o$. R_{free} is calculated as R, but for 10% of the reflections excluded from all refinement. The R_{free} set was chosen in thin shells due to the 3-fold non-crystallographic symmetry

[d] Percentage of residues in the most favored, additionally allowed, generously allowed, and disallowed regions of a Ramachandran plot.

Figure S1

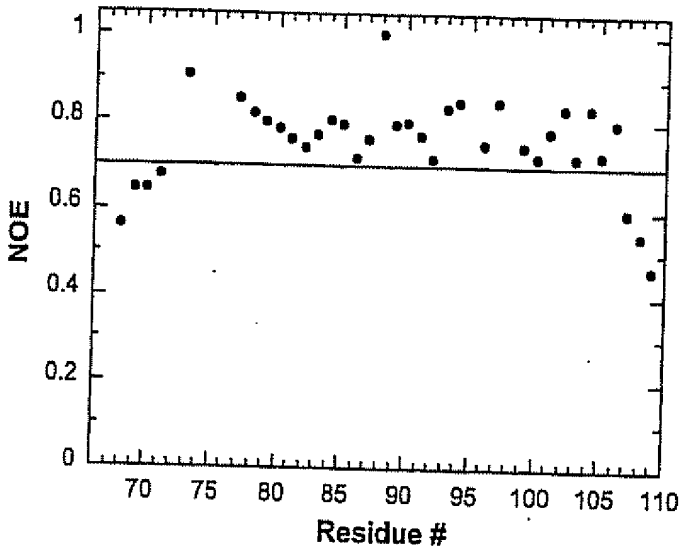

Figure S1. Heteronuclear NOE values for TACI_d2. Steady-state ^{1}H-^{15}N heteronuclear NOE values are plotted as a function of residue number. Absence of a symbol indicates the presence of proline or a residue whose amide resonance was not observed. NOE values were calculated as the ratios of peak heights in the spectra recorded with (NOE) and without (no NOE) proton saturation. NOE values below dotted line indicate that these residues are highly dynamic on the picosecond-nanosecond time scale.